Hybrid Energy Storage System of an Electric Scooter Based on Wireless Power Transfer

Jia-Sheng Hu, *Senior Member, IEEE*, Fei Lu, *Member, IEEE*, Chong Zhu, *Member, IEEE*, Chang-Yi Cheng, Sin-Li Chen, Tsai-Jiun Ren, and Chunting Chris Mi, *Fellow, IEEE*

***Abstract*—The aim of this paper is to present the design and implementation of a hybrid energy storage system (HESS) with wireless power transfer (WPT). This study combines a battery bank and a supercapacitor bank to achieve high performance energy sources for electric scooters. The proposed system can be employed on commercial 48-V electric scooters for evaluation. The presented approach follows the WPT frequency standard of SAE J2954 to build the energy transmission. Based on the control of the state of charge on the battery bank, this paper proposes a three-mode strategy for hybrid energy management. The proposed HESS makes three compact and integrated contributions. First, it acts as the regulator to manage the input energy from WPT. Second, it manipulates the energy distributions to the battery and supercapacitor. Third, it provides a mechanism to initiate a short period of "negative current" to avoid excessive exploitation of the battery and facilitates palliation upon polarization. This function has the ability to extend battery life. The system performance of the electric scooter, as a result, can be improved. A double-sided *LCC* coil with a 15-cm air gap for wireless charging was built on a 0.8-kW electric scooter. In the wireless stage, the efficiency from the dc source to the dc output after the rectifier is 90.362%. The overall system efficiency from the dc source to the battery and supercapacitor is 86.4%.**

***Index Terms*—Electric scooter, hybrid energy storage system (HESS), *LCC* topology, resonant frequency, wireless power transfer (WPT).**

Manuscript received September 29, 2017; revised December 16, 2017 and January 26, 2018; accepted February 11, 2018. Date of publication February 16, 2018; date of current version September 4, 2018. This work was supported by the Ministry of Science and Technology (MOST) of Taiwan, under Projects MOST 106-2221-E-024-013 and MOST 106-2918-I-024-003. Paper no. TII-17-2268. *(Corresponding author: Jia-Sheng Hu.)*

J.-S. Hu is with the Department of Greenergy, National University of Tainan, Tainan 700, Taiwan (e-mail: jogson@ieee.org).

F. Lu, C. Zhu, and C. C. Mi are with the Department of Electrical and Computer Engineering, San Diego State University, San Diego, CA 92182 USA (e-mail: feilu@umich.edu; chong.zhu@sdsu.edu; cmi@sdsu.edu).

C.-Y. Cheng is with the Department of Electrical Engineering, National Cheng Kung University, Tainan 701, Taiwan (e-mail: s9003794@gmail.com).

S.-L. Chen is with the Rich Electric Corporation Limited, Tainan 702, Taiwan (e-mail: air150181@gmail.com).

T.-J. Ren is with the Department of Information Engineering, Kun Shan University, Tainan 710, Taiwan (e-mail: cyrusren@mail.ksu.edu.tw).

Color versions of one or more of the figures in this paper are available online at http://ieeexplore.ieee.org.

Digital Object Identifier 10.1109/TII.2018.2806917

I. Introduction

UNLIKE internal combustion engines, which cause environmental problems, such as air pollution and global warming, the operation of an electric motor is zero emission. Therefore, the electric vehicle (EV) appears to be one of the best options for public transportation [1]–[2]. The battery is a suitable platform to support the progress of EVs because of its high energy density and mobility. Most commercial batteries produce electricity via electrochemical reactions, which gradually decay because the polarization mechanism causing the chemical reaction is restricted [3]–[6]. Usually, the performance and lifetime of the battery quickly decline because of the often high-current charge and discharge. Consequently, it is difficult to maintain the system performance after several instances of full charging and discharging. Conversely, unlike the battery, which produces energy via electrochemical reactions, the supercapacitor (SC) creates energy differently. The SC stores the electric potential via a physical mechanism of the electric field. As a power source, the energy density of the SC is not on par with its lengthy lifetime. The differences between the battery and SC as energy sources have been investigated in many studies, such as [7]–[9]. Fig. 1 summarizes the quantitative comparisons between the battery and SC [8]. As can be seen in Fig. 1, the power density and lifetime between these two elements are clearly different. In the battery- SC combined system, the excessive charge/discharge current can be provided by the SC during some transients, such as rapid regenerative braking or accelerating, while the normally operation power is still sustained by the battery. In this way, the battery is free from the overlarge charge/discharge current without using an SC of massive capacitance and volume. Hence, using the hybrid policy to compensate each other can enlarge the whole area of radar chart. If we can sufficiently use both of these two energy sources, the system performance of EVs can be improved. Based on the merits of proper hybrid compensation, the high-power output and long-life battery can be achieved at the same time.

Generally, not all forms of urban transportation require high speed and endurance. Hence, the demand for light EVs, such as electric scooters, is increasing [10]. Compared to other EVs, the electric scooter has a good weight-propulsion rate. In addition, it is compact, nimble, highly efficient, and more cost effective than other electric counterparts. Hence, it has gradually become the first choice for short distance (less than 30 km) transportation. Similar to the other EVs, the performance of the electric scooter is mainly dominated by the battery. In order to improve

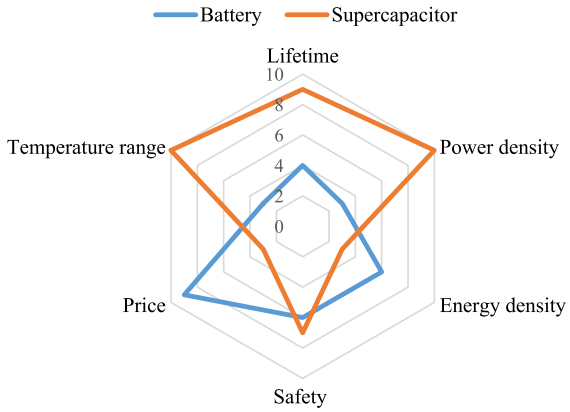

Fig. 1. Quantitative comparisons: Battery versus SC.

the performance of the conventional electric scooter, this paper utilizes both the battery and SC to build the energy sources for propulsion. Basically, the SC can offer high-current output to cover the battery as the electric scooter needs torque for acceleration in a short time. The battery can supply the required energy during cruise control, and the hybrid policy between the components protects the battery from becoming seriously damaged. Therefore, the power management system reveals its importance. Herein, the management system of the dual energy source can also be referred as the hybrid energy storage system (HESS) [11]. According to [11], HESS can break through the application barrier from a single battery. An HESS can potentially form an economical, sustainable solution to power systems.

Regarding the dual energy charging design for EVs, many approaches have been studied. Basically, the dual source system can provide efficient regenerative braking, better battery safety, and nimble vehicle acceleration. In [8], a regenerative braking system based on an integrated buck converter is implemented in EVs. A WPT system with a simple charger is proposed for light EVs with SC storage in [12]. A multiport, isolated, bidirectional dc–dc converter for hybrid battery and SC applications is proposed in [13], which can achieve zero voltage switching for all switches in the whole load range. In the viewpoint of [14], the real-time load dynamics for computing the SC reference voltage reveals its importance. Hence, they propose a two-stage power control framework to deal with the real-time power optimization. From the radar chart of Fig. 1, we know that the SC and battery are complementary power sources. Obviously, in order to balance the dual energy sources for system control, the management of energy distribution via HESS is crucial. Additionally, HESS is always playing an important role on balancing and optimization not only for EV applications, but also for renewable energy grids [15]–[16]. Regarding the automatic power regulations, control methodologies, such as model predictive control [17], adaptive sliding-mode with hysteresis control [18], neural networks [19], and fixed-frequency sliding mode control [20], have been employed. For the quantitative analysis and modeling of the HESS, readers can refer to [21].

Regarding the difference between proposed approach and related works [8]–[10], [12]–[13], the presented approach provides an integrated solution to build the HESS for the electric scooter. The whole circuit contains the dc source/inverter, WPT unit, rectifier, HESS, load side inverter, and motor. Comparing to [8]–[9], [12]–[13], the switching strategy is not the same. Three major contributions of proposed approach are highlighted.

1) It acts as the regulator to manage the input energy from WPT.
2) It manipulates the energy distributions to battery and SC.
3) It provides a mechanism to initiate a short "negative current" period to avoid excessive exploitation of the battery and facilitates palliation upon polarization. This function has the ability to extend battery life.

First, the conventional WPT unit needs a dc–dc converter either before the primary coil or after the secondary circuit. While, in the hybrid energy storage, there is no need for an extra dc–dc converter to handle the energy to the major dc bus. Because it manages the power/energy between the battery and SC using its exclusive converter. This paper proposes a novel design that regulates the input power from WPT efficiently. Second, the presented circuit integrates multiple functions into a concise HESS, which contains three operation modes, i.e., rapid, normal, and smart ones. It manipulates the energy distributions between each energy storage units via the three-mode strategy. The presented methodology releases certain extreme electrochemical reactions in the battery pack while a heavy current is pursued. Third, according to the investigations in [3] and [5], during the charging process, the positive and negative pulse of the charging current can be applied to pull the electrolytic ions away from electrode. This mechanism also refers to depolarization pulse in [6], which is applied to reduce the increase of the internal resistance of the battery due to severe concentration polarization. Because of the regulation of the depolarization mechanism, the temperature rise of battery can be slightly released. Basically, the depolarization pulse is used to decrease the concentration gradient, the depolarization pulse should not cause any significant discharge of the battery. Moreover, existing battery charging strategies typically do not take into account the electrochemical properties of batteries, because these factors are difficult to obtain during charging operation. From the report of [22], the sinusoidal ripple current charging algorithm is feasible to reduce the activation polarization of Li-ion battery. At the optimal frequency, the ac impedance of a battery can be minimized. Consequently, a short "negative current" period in the dc–dc charging stage can release the polarization on electrodes and maintain strong battery performance and its lifetime. This paper proposes a novel, three-mode HESS, which was proved in experiments in which a short period of negative current had been truly initiated.

II. Wireless Power Transfer

For electric scooters, wire-connected charging is always an inconvenient issue. The drawbacks are as follows.

1) The charger plug is not unified.
2) The wire is at risk of giving an electric shock.
3) The wire has the potential to be twisted.

Furthermore, the performance limitations for the electric scooter are the following.

1) Due to the cabin constraint, the capacity of the battery is often small, e.g., 1 kWh, requiring frequent recharging. For a common charger, the wait time is long, and the number of plugs for specific battery chargers is insufficient.

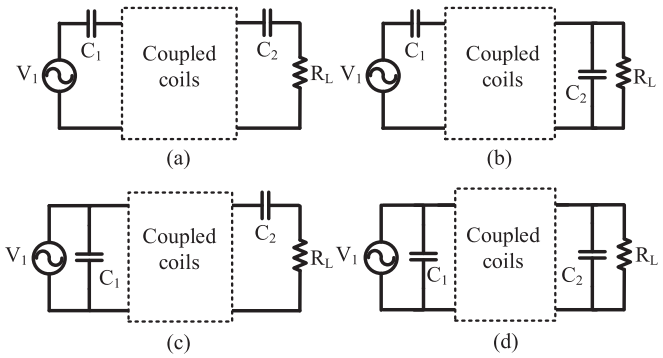

Fig. 2. Four basic topologies. (a) SS (b) SP (c) PS (d) PP.

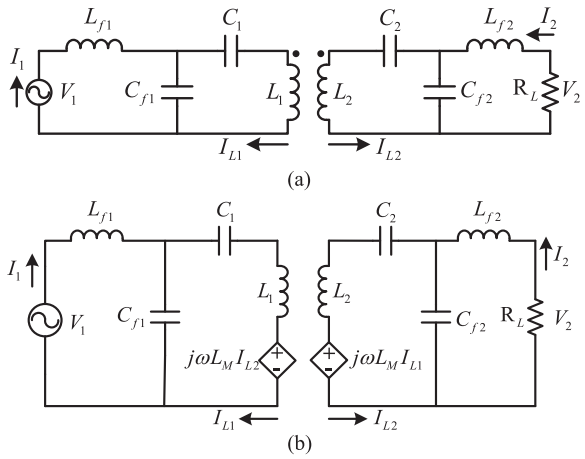

Fig. 3. Double-sided *LCC* compensation topology. (a) Double-sided *LCC* resonant circuit. (b) Equivalent circuit.

2) The limitation of the battery constrains the output torque of the electric motor because the battery cannot supply extra current when instantaneous torque is needed.

Consequently, wirelessly charging electric scooters is of interest. Wireless charging for EV has become a trend due to its safe operation and convenience [23]. In this paper, an electric scooter with the functions of WPT and HESS will be proposed. Related issues about WPT will be discussed in this section.

Regarding wireless power transfer, many approaches are referenced and studied, such as, magnetic flux induction, two-coil loosely coupled transformer, microwave, and lasers [24]–[25]. Herein, the two-coil loosely coupled transformer, which can transfer power wirelessly with high efficiency across large air gaps is of note. As shown in Fig. 2, four basic topologies are often referenced. Depending on how the compensation capacitors are added to the transmitting and receiving coils, they are simply named as series–series (SS), series–parallel (SP), parallel–series (PS), and parallel–parallel (PP) topologies [26]–[28]. A more recent compensation topology, known as the double-sided *LCC* compensation topology [29]–[30], shows its benefits in high power WPT. As illustrated in Fig. 3(a), this topology consists of one inductor and two capacitors at both the primary and secondary sides. Note that in Fig. 3(a), the double-sided *LCC* compensation topology was applied in the WPT unit of this paper. Comparing to the four basic WPT topologies in Fig. 2, the main advantage of the *LCC* compensation circuit is that the output power is proportional to the coupling coefficient, which is convenient in a practical application. For example, in an *LCC*-compensated system, when the receiver has misalignment with the transmitter, the system power is decreased. However, in an SS-compensated system, the system power can be significantly increased, which could cause danger.

From Fig. 3(a), the equivalent circuit can be obtained as Fig. 3(b). The circuit in Fig. 3(b) can be described by the following equations:

$$\begin{bmatrix} V_1 \\ 0 \\ 0 \\ 0 \end{bmatrix} = \begin{bmatrix} a & \frac{-1}{j\omega C_{f1}} & 0 & 0 \\ \frac{-1}{j\omega C_{f1}} & b & j\omega L_M & 0 \\ 0 & j\omega L_M & c & \frac{-1}{j\omega C_{f2}} \\ 0 & 0 & \frac{-1}{j\omega C_{f2}} & d \end{bmatrix} \begin{bmatrix} I_1 \\ I_{L1} \\ I_{L2} \\ I_2 \end{bmatrix}, \quad (1)$$

where

$$a = j\omega L_{f1} + \frac{1}{j\omega C_{f1}}, b = \frac{1}{j\omega C_1} + \frac{1}{j\omega C_{f1}} + j\omega L_1$$

$$c = \frac{1}{j\omega C_2} + \frac{1}{j\omega C_{f2}} + j\omega L_2, d = j\omega L_{f2} + \frac{1}{j\omega C_{f2}} + R_L. \quad (2)$$

Note that $L_M = k\sqrt{L_1 L_2}$ stands for the mutual inductance and k is the coupling coefficient. Basically, the resonance can be obtained in many ways. The useful conditions are obtained when all the diagonal elements are real and no imaginary part is present. Thus, the following resonant conditions can be derived

$$\omega^2 L_{f1} C_{f1} = \omega^2 L_{f2} C_{f2} = 1$$
$$\omega^2 (L_1 = L_{f1}) C_1 = \omega^2 (L_2 - F_{f2}) C_2 = 1. \quad (3)$$

Clearly, the resonant frequency ω should be controlled under the condition of

$$\omega = \frac{1}{\sqrt{L_{f1} C_{f1}}} = \frac{1}{\sqrt{L_{f2} C_{f2}}}$$
$$= \frac{1}{\sqrt{(L_1 - L_{f1}) C_1}} = \frac{1}{\sqrt{(L_2 - L_{f2}) C_2}}. \quad (4)$$

Then, under this resonant condition, the resonant frequency of (4) is only related to inductances and capacitances, independent of coupling and the load condition. Additionally, (1) can be further simplified as

$$V_1 = \frac{-1}{j\omega C_{f1}} I_{L1}, 0 = \frac{-1}{j\omega C_{f1}} I_1 + j\omega L_M I_{L2}$$
$$0 = j\omega L_M I_{L1} + \frac{-1}{j\omega C_{f2}} I_2, 0 = \frac{-1}{j\omega C_{f2}} I_{L2} + R_L I_2. \quad (5)$$

Substituting the condition of (2) into (5), the output current I_2 can be expressed as

$$I_2 = \frac{jL_M}{\omega L_{f1} L_{f2}} V_1. \quad (6)$$

For a resistive load, its output voltage V_2 is in phase with output current (I_2); therefore, the delivered power can be

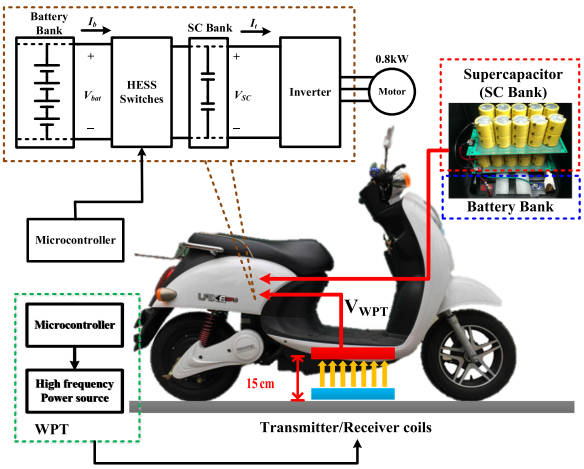

Fig. 4. Proposed WPT electric scooter. (a) System scheme of proposed scooter. (b) Dimension of transmitter/receiver coils.

expressed as

$$P = |I_2|\,|V_2| = \frac{L_M}{\omega L_{f1} L_{f2}}\,|V_1|\,|V_2| = {I_2}^2 R_L. \tag{7}$$

III. Proposed Approach

As mentioned in the Introduction, this paper proposed an electric scooter system with dual energy sources. Both the battery and SC are installed in the scooter to enhance the dynamic performance of the original system. Fig. 4 demonstrates the system scheme and coils for WPT of the proposed electric scooter. The air gap between transmitter and receiver coils is 15 cm. The WPT coils [see Fig. 4(b)] are square with a side length of 12 inches (30.5 cm). The major function of the SC and battery are energy sources. Considering to the same scooter applications in [10], its electric scooter is powered by a fuel cell system with the assistance of an SC bank. Although the energy storage system is both hybrid, the circuit implementation is quite different between the proposed approach and [10]. This paper adopts the *LCC* topology to set up the WPT system, i.e., Fig. 3. Comparing to the SS WPT approach for light EV in [12], the transferred power of an *LCC*-compensated WPT system is proportional to the coupling coefficient.

It is mentioned that the battery exerts energy via an electrochemical reaction, whereas the SC stores energy by electric potential. The SC has extraordinarily high power density, and it compensates the lifetime problem of batteries on high current charge or discharge. The output of its power density is ten times higher than that of a general lead-acid battery. Clearly, the major advantage of the SC is its rapid response and long lifetime. However, compared to batteries, its energy density is still too low. In addition, disadvantages, such as high cost, low voltage, and faster self-discharge, still constrain its applications. The proposed HESS combines both the battery and SC together to comprise the output power of the system. Therefore, the dynamic performance, such as quick start and nimble acceleration, can be achieved for the proposed scooter. Additionally, the lifetime of the battery can be extended because the SC compensates most of the deep charging/discharging tasks from the battery in the operation period. Consequently, the battery can initiate better electrochemical reactions.

As mentioned in the Introduction, a three-mode strategy was proposed in this study. Fig. 5 is the proposed flowchart of the systematic operation mode. Herein, $V_{\rm SC}$ and $V_{\rm bat}$ stand for the voltage level of SC and battery, respectively. $I_{\rm SC}$ is the current of the SC. As can be seen in Fig. 4(a), the power source for the proposed HESS comes from the WPT. The energy is then transferred from ac to dc via a rectifier and boost/buck converters to achieve the required voltage and current levels. Generally, as shown in Fig. 5, the presented approach makes the decisions by reading the state of charge (SOC) of the battery and SC. After acquiring the SOC information from the battery and SC, the system switches to the relevant mode to control the power switches. The switching modes contain the following:

1) rapid charging;
2) normal charging; and
3) smart charging.

The main circuit of the proposed HESS is shown in Fig. 6. Note that $V_{\rm WPT}$ is the dc voltage coming after the rectifier of the secondary WPT coils. The major energy is stored in the battery, and the SC contributes while specific operations are underway. Indeed, different modes facilitate different power flows according to various scenarios.

A. Rapid Charging Mode

According to Fig. 5, the tested electric scooter faces a "rapid charging" mode, while the voltage of the SC is lower than the battery. Fig. 7 illustrates the designate energy flow. In this condition, all the switches ($S_1 - S_4$) in full-bridge are turned OFF, and all the relays ($R_{y1} - R_{y3}$) are still inactive. Therefore, at this stage, the system will install all input energy into the SC. The purpose is to charge the SC using an extremely high current. Regarding the stored energy in the SC, the following equation can be found

$$U = \int_{q_i}^{q_f} \frac{q}{C} dq. \tag{8}$$

Herein, U is the energy stored in the SC, and C is the capacitance. Due to that the energy in (8) is easy to build up, this mode will not be activated for some time.

B. Normal Charging Mode

When the SC voltage reaches the specific voltage level, the system operates in the "normal charging" mode. As shown

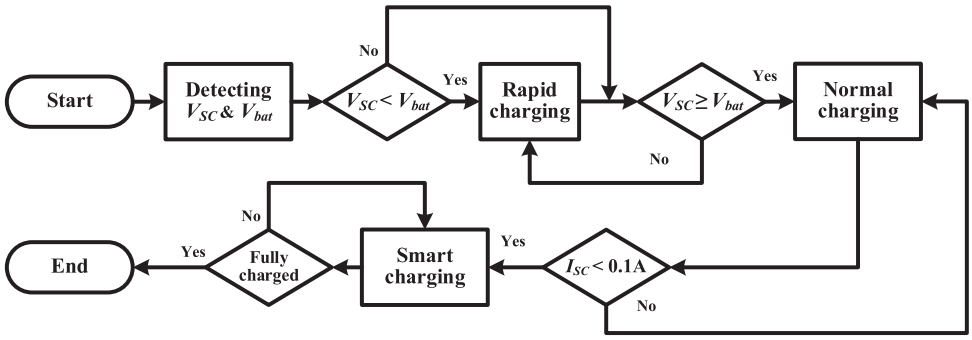

Fig. 5. Flowchart of the proposed HESS.

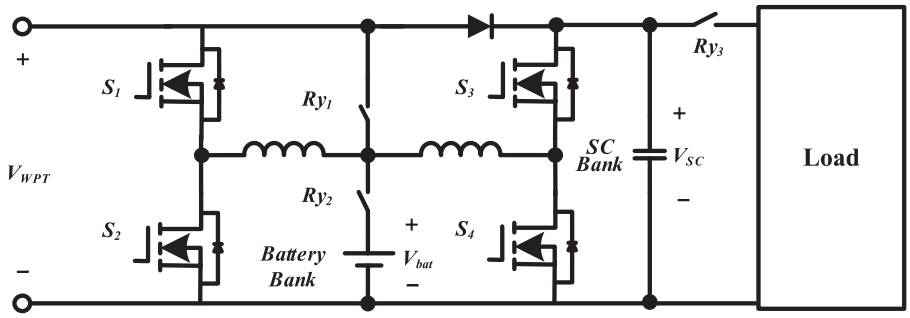

Fig. 6. Circuit of the proposed HESS.

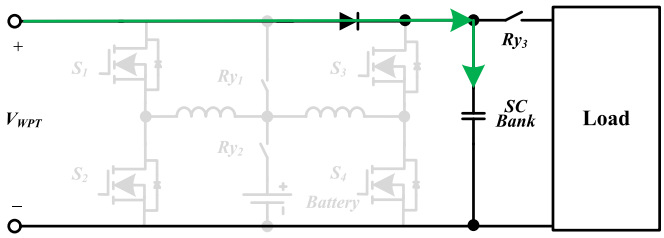

Fig. 7. Energy flow of rapid charging mode.

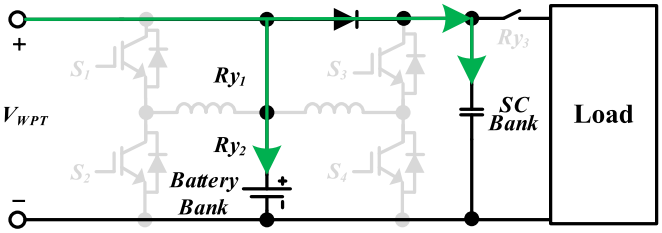

Fig. 8. Energy flow of normal charging mode.

in Fig. 8, all switches ($S_1 - S_4$) are inactive, and relays ($R_{y1} - R_{y2}$) are activated. The system transfers the power to battery and SC at the same time. Basically, the current from WPT is distributed according to the electric potential and electrical impedance of the battery and SC. When the voltage of the SC rises, it decreases its charging current so that the charging current of the battery will increase simultaneously. The following equation shows the relevant current distribution:

$$I_{\mathrm{WPT}}(t) = I_{\mathrm{bat}}(t) + I_{\mathrm{SC}}(t). \tag{9}$$

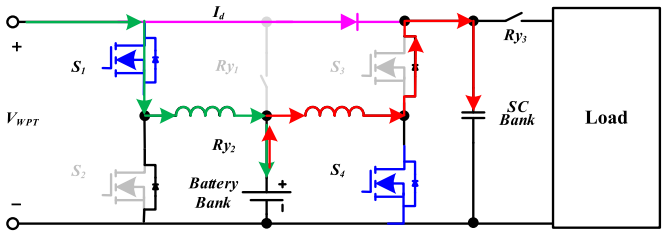

Fig. 9. Energy flow of smart charging mode.

Herein, I_{WPT} is the WPT current; I_{bat} and I_{SC} are current distributed in the battery and SC. When the SOC of SC is high, most of the charging current will go into the battery.

C. Smart Charging Mode

According to the investigations in [3] and [5], during the charging process, the positive and negative pulse of charging current can be applied to pull the electrolytic ions away from electrode. Consequently, the short "negative current" period in the dc–dc charging stage can release the polarization on electrodes and maintain strong battery performance and its lifetime. In this paper, a similar idea was realized in our "smart charging" mode. When the voltage of the SC reaches the rating charging voltage, the charging current of the SC is much lower than the battery. Then, the system operates in the "smart charging" mode. The switching strategy is shown in Fig. 9. In this mode, 80% of the processing time is utilized for buck charging on the battery bank, and the remaining time (20%) is employed for

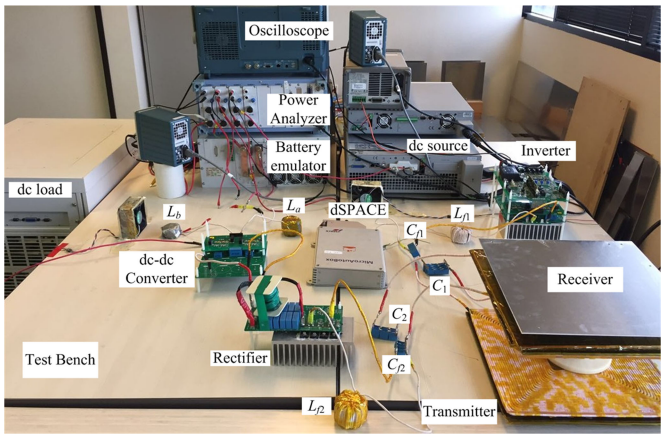

Fig. 10. Test bench of the experiments.

boost charging on the SC bank. The current of I_d (the purple line) coming from the WPT coil charges the SC bank during the entire cycle. Note that, in this mode, relay R_{y2} is always on and R_{y1} and R_{y3} are always OFF. That is, in the first 80% of the process period, the WPT current charges the battery by merely switching S_1 ON (the green line). Then, for the remaining 20% of the process period, S_1 is tuned OFF, and S_4 is turned ON instead (the red line). In the short 20% period, the battery uses the stored current in the inductor to charge the SC as a boost converter. The connection between the battery and the SC is the Schottky diode. It helps to prevent the SC from recharging the battery by the difference in voltage. In the proposed smart charging, the SC bank can be charged with extra energy from the inductor, which is powered by the battery bank. Additionally, the battery bank charges (80%) and discharges (20%) in one processing cycle. This mechanism provides a "negative current" to avoid the excessive exploitation of the battery and facilitates palliation upon polarization. Obviously, the battery's performance can be maintained in consequence.

IV. Experimental Test Bench and Electric Scooter

The experimental evaluations are divided into two stages. First, the verification experiments are carried out on the test bench (see Fig. 10). Then, the experiments for the second stage are tested on the real scooter. For the sake of implementing the proposed algorithm, a microcontroller (dSPACE 1401/1501) was employed. The dSPACE 1401/1501 is used to generate complementary control signals of the buck and the boost converters, whose duty ratios are D and 1-D, respectively. The dead time of the pulse-width-modulation (PWM) signals is set to 1 μs, whose effect can be neglected considering a pulse period of 0.1 ms. During the battery charging process, the duty ratio of the PWM signals is gradually adjusted according to the proposed battery charging algorithm.

The WPT frequency of 85 kHz is set up by the inverter from the dc source side. The dc-link voltage of the H-bridge inverter is supplied by a dc power source. Two channels of complementary 85-kHz PWM signals, whose duty ratio is 0.5, are generated by the TMS320F28335-based DSP board. Then, the MOSFETs of the inverter are driven by the PWM signals from the DSP board to generate the square wave voltages.

TABLE I
Vehicle Specification

Specification	Value
Motor power	0.8 kW
Max speed	40 km/h
Size	165 × 25 × 37 cm
Maximum payload	100 kg
Inverter voltage range	41∼65 V
Battery Bank	Lead-acid battery × 4 (12 V/10 Ah, up to 54 V)
SC Bank	27 V 40 F module × 2

TABLE II
Specifications of the Experiments

DC source	100 V/8 A
Capacity of battery bank	48 V/11 AH
Capacity of SC bank	81 V/13.33 F
Inductor of L_1	270 μH
Inductor of L_{f1}	31 μH
Capacitor of C_1	14.0 nF
Capacitor of C_{f1}	156.3 nF
Inductor of L_2	270 μH
Inductor of L_{f2}	22.3 μH
Capacitor of C_2	14.8 nF
Capacitor of C_{f2}	110.5 nF
Inductor of L_{h1}	60 μH
Inductor of L_{h2}	60 μH
Mutual inductance L_M	49.1 μH
Air gap between WPT coils	15 cm

For real scooter testing, a prototype electric scooter, namely Laike-mini [see Fig. 4(a)], was employed to carry out the experiments. Table I illustrates the relevant specifications of Laike-mini. Its rated dc voltage is 48 V, which is a common specification in the market.

V. Experimental Examples and Discussion

Fig. 11 shows the whole circuit of the proposed system. In the HESS experiments, the PWM frequency is set to 10 kHz. Specifications of the proposed circuits can be found in Table II. Experiments are both carried out on the test bench and the prototype electric scooter, respectively.

To eliminate the conductive loss induced by skin effect, Litz-wire is used to build the inductors and main coils. At 85 kHz, the skin depth of copper is 223.6 μm, and an 800-strand AWG 38 wire with 100-μm diameter is used in this design. The main coil has 30 turns to achieve the inductance value of 270 μH. To further reduce the power loss in the semiconductor devices, silicon carbide (SiC) MOSFET (C2M0025120D) from CREE is used in this design, and its equivalent turn-on resistance is only 25 mΩ. For the diode, SiC device (C3D20060D) from the same manufacturer is used.

A. Evaluations on Test Bench

First experiment is the performance evaluation on WPT. Fig. 12 shows the experimental results. Fig. 12(a) illustrates the efficiency results. The WPT unit can achieve an efficiency of

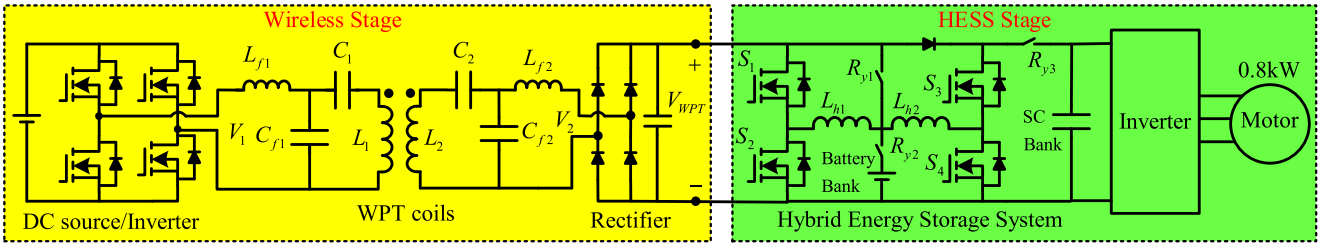

Fig. 11. Schematic system of wireless charging for HESS of proposed scooter.

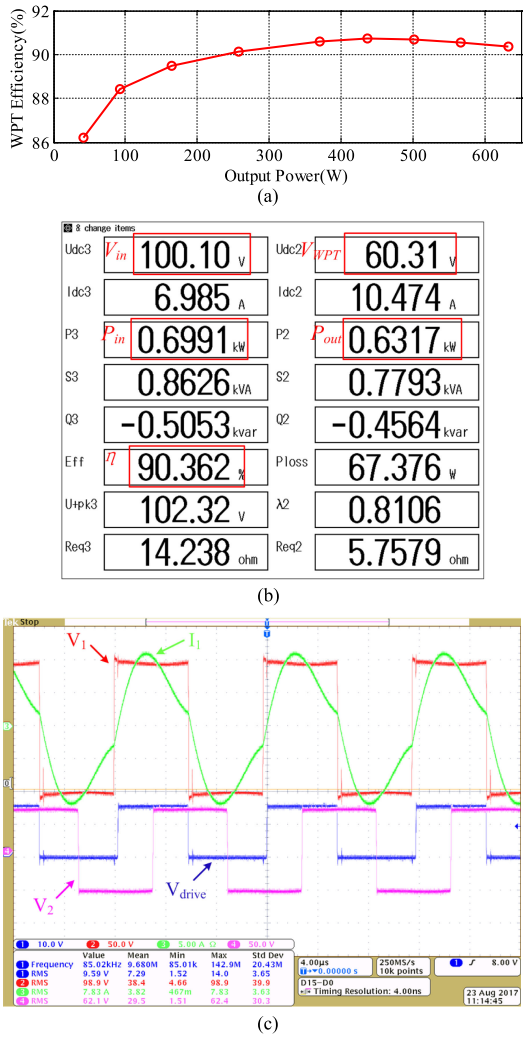

Fig. 12. Experimental results for WPT evaluation. (a) WPT efficiency. (b) Results from power analyzer. (c) Waveform of the testing.

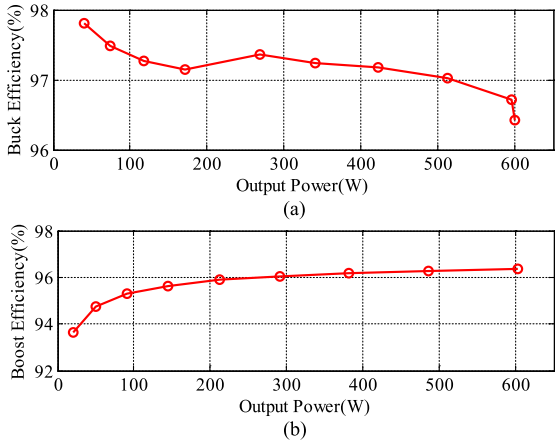

Fig. 13. Experimental results for buck and boost converter. (a) Buck efficiency. (b) Boost efficiency.

90.362% from the dc input voltage to the dc output of the rectifier on the output power of 631.7 W. The relevant results are measured by a power analyzer as illustrated in Fig. 12(b). Note that the WPT input is controlled as the condition of $V_{\mathrm{WPT}} = 60\,\mathrm{V}$. Fig. 12(c) shows the waveform of the WPT experiments. V_1 is the ac excitation voltage to the resonant circuit at the primary side, and V_2 is the ac voltage before rectifier at the secondary side. Clearly, the operation frequency of the proposed system is falling on the nominal value of 85 kHz. This result confirms that the proposed system follows the frequency standard of SAE J2954. In addition, the proposed WPT unit can achieve zero voltage switching. Fig. 13 gives the experimental results for buck and boost converter. As can be seen in this figure, the efficiency of the buck and boost converters are both over 95%. Fig. 14 shows the experimental results of the smart charging mode. This is an important mode that can initiate the triangular and negative current of the battery to achieve depolarization. In this mode, 80% of the cycle time was employed for the buck converter, and the rest 20% was used for the boost converter. Fig. 14(a) shows the efficiency of this mode. Fig. 14(b) demonstrates the relevant waveforms of the experiment. As can be seen in this figure, the triangular and negative current (I_{bat}) of the battery can be observed. This means that the depolarization mechanism is well posed. In the proposed approach, the rapid charging mode shares some current distribution from the battery. The smart charging mode prevents deep polarization of the battery. Hence, the lifetime and performance of the proposed system can be further guaranteed. Fig. 15 summarizes some comparative results. Clearly, the overall system efficiency from the dc source to the battery and SC is 86.4% on the output power of 596 W.

B. Evaluations on Prototype Electric Scooter

In the following, the charging tests are carried out on the prototype electric scooter. First, the rapid charging mode is verified. In this mode, the system proceeds to quickly charge the SC via WPT. Note that in this mode, the voltage of the SC

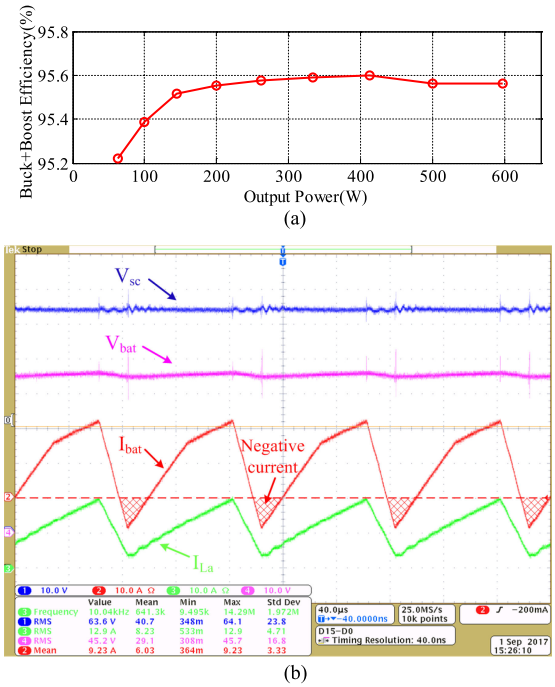

Fig. 14. Experimental results for smart charging mode. (a) Efficiency. (b) Waveform of the testing.

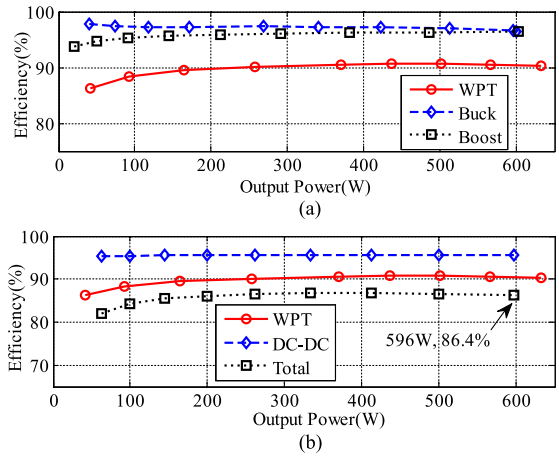

Fig. 15. Experimental results for smart charging mode. (a) Comparative results I. (b) Comparative results II.

is lower than that of the battery. Fig. 16 shows the experimental current–voltage curves of the SC in rapid charging mode. As can be seen in this figure, the whole energy from WPT enters the SC during the process. The operating mode switches to the normal charging mode. The battery and SC are then charged for a while during this mode. Fig. 17 reveals the current and voltage of the normal charging mode. In this mode, WPT energy enters the battery and SC, respectively. In addition, in this mode, the SC also acts as the low-pass filter to relax the electrochemical reaction. In this figure, an interesting phenomena can be observed. Basically, from the proposed flowchart of Fig. 5, the active condition of the normal charging mode is $V_{\mathrm{SC}} \geq V_{\mathrm{bat}}$. Consequently, in the beginning of this mode, most of the

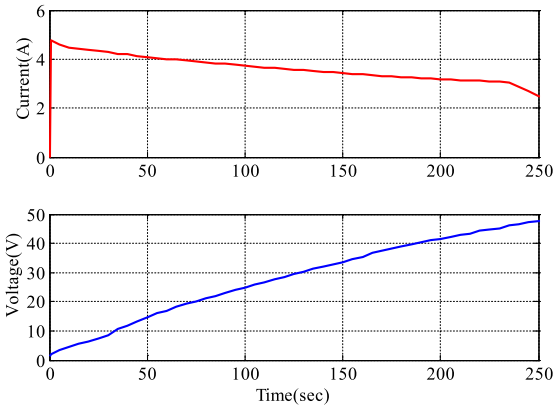

Fig. 16. Experimental current–voltage curves of SC in rapid charging mode.

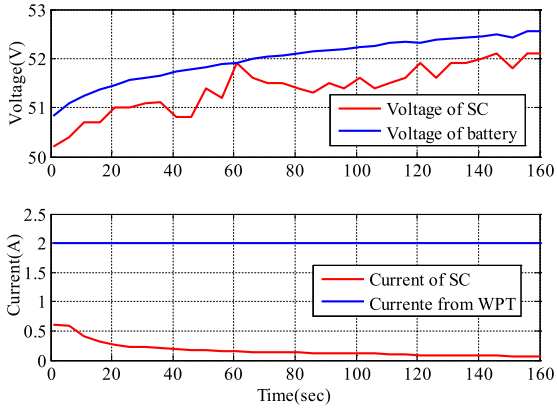

Fig. 17. Experimental charging status of normal charging mode.

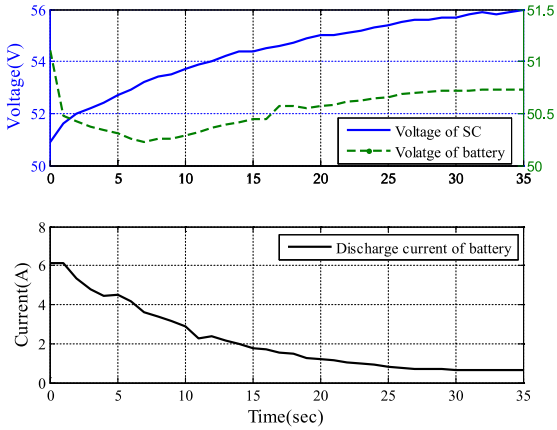

Fig. 18. Experimental results in smart charging mode.

current from the WPT will enter the battery to increase its electric potential.

Finally, after the high power demand mode is passed, the system will then be switched to the smart changing mode. This is the final stage of battery charging. After this mode, the battery will be fully charged. Basically, the buck/boost ratio of smart charging mode can be flexibly adjusted. In this mode, the depolarization mechanism offers a specific recovery for battery to maintain its lifetime and performance. Fig. 18 gives the

experimental results. In this mode, the boost converter charges the SC, which makes the voltage of the SC higher than the battery. Without the booster converter, the overall voltage level will be constrained by the battery. By applying the booster converter, the energy stored in the battery can be further transfer to the SC. Consequently, the overall storage rate of SC can be increased. Due to the minute energy transfer, the voltage level of battery will drop a bit during the booster charging period. Due to that the energy density of the SC is small, the battery voltage drops slightly during this operation. In addition, the battery current registers a small value in the steady state. Because of the precise internal resistance of the battery model is not a constant [6], [11], it will vary slightly depending on the current demands. Therefore, the voltage profile of battery will increase a bit due to lighter load requests. As can be seen in Fig. 18, from 0–10 s, the current demand is large, the electrochemical reaction is strong and the internal resistance slightly increased, causing a small voltage drop. From 10–25 s, the current request is small, and the voltage rises a bit in consequence. After 25 s, the current demands reach steady state, and the voltage profile keeps the same voltage level.

VI. Conclusion and Future Work

This study has proposed an energy management strategy of HESS, which is powered by WPT. It is suitable for commercial 48-V electric scooters. The operation frequency of WPT is 85 kHz, which follows the frequency regulations of SAE J2954. A double-sided *LCC* coil with a 15-cm air gap for wireless charging has been built on a 0.8-kW electric scooter. At the wireless stage, the efficiency from the dc source to the dc output after the rectifier is 90.362%. The overall system efficiency from the dc source to the battery and SC is 86.4%. In the presented HESS circuit, this paper has presented a three-mode strategy for realizing the claimed functions. The experimental results confirmed the feasibility of the proposed strategy. Moreover, the study has verified that the proposed HESS and control strategy can improve the performance of a common electric scooter. It not only improves the performance of the battery, but also has the ability to extend the lifetime of the whole energy system.

This paper focuses on the wireless charging for the proposed HESS, aiming at providing a better power distributing between the battery and the SC as well as extending the battery life. Regarding the future work of this study, the rectifier circuit should be upgraded to an active one. Hence, the discharging and regenerative braking functions can be applied. About the depolarization function, a series of experimental evaluations upon the improvement issue of lifetime should be carried out. In addition, considering to the dynamic charging, the compensation circuit for *LCC* topology should be improved. Then, the whole system could gain more benefits from more flexible operations.

References

[1] Y. Hori, "Looking at cars 100 years in the future," in *Proc. 2013 IEEE Int. Conf. Mechatronics*, Vicenza, Italy, 2013, pp. 31–35.

[2] J. S. Hu, Y. Wang, H. Fujimoto, and Y. Hori, "Robust yaw stability control for in-wheel motor electric vehicles," *IEEE/ASME Trans. Mechatronics*, vol. 22, no. 3, pp. 1360–1370, Jun. 2017.

[3] P. H. Cheng and C. L. Chen, "High efficiency and nondissipative fast charging strategy," *IEE Proc.-Elect. Power Appl.*, vol. 150, no. 5, pp. 539–545, 2003.

[4] S. T. Hung, D. C. Hopkins, and C. R. Mosling, "Extension of battery life via charge equalization control," *IEEE Trans. Ind. Electron.*, vol. 40, no. 1, pp. 96–104, Feb. 1993.

[5] X. Gong, "Modeling of lithium-ion battery considering temperature and aging uncertainties," Ph.D. dissertation, Automotive Syst. Eng., Univ. Michigan–Dearborn, Dearborn, MI, USA, 2016.

[6] S. C. Kim and W. H. Hong, "Fast-charging of a lead–acid cell: Effect of rest period and depolarization pulse," *J. Power Sources*, vol. 89, no. 1, pp. 93–101, 2000.

[7] J. M. Blanes, R. Gutiérrez, A. Garrigós, J. L. Lizán, and J. M. Cuadrado, "Electric vehicle battery life extension using ultracapacitors and an FPGA controlled interleaved buck–boost converter," *IEEE Trans. Power Electron.*, vol. 28, no. 12, pp. 5940–5948, Dec. 2013.

[8] F. Naseri, E. Farjah, and T. Ghanbari, "An efficient regenerative braking system based on battery/supercapacitor for electric, hybrid, and plug-in hybrid electric vehicles with BLDC motor," *IEEE Trans. Veh. Technol.*, vol. 66, no. 5, pp. 3724–3738, May 2017.

[9] B. Wang, J. Xu, R. J. Wai, and B. Cao, "Adaptive sliding-mode with hysteresis control strategy for simple multimode hybrid energy storage system in electric vehicles," *IEEE Trans. Ind. Electron.*, vol. 64, no. 2, pp. 1404–1414, Feb. 2017.

[10] M. Bertoluzzo and G. Buja, "Development of electric propulsion systems for light electric vehicles," *IEEE Trans. Ind. Informat.*, vol. 7, no. 3, pp. 428–435, Aug. 2011.

[11] X. Hu, C. Zou, C. Zhang, and Y. Li, "Technological developments in batteries: A survey of principal roles, types, and management needs," *IEEE Power Energy Mag.*, vol. 15, no. 5, pp. 20–31, Sep./Oct. 2017.

[12] Z. Li, C. Zhu, J. Jiang, K. Song, and G. Wei, "A 3-kW wireless power transfer system for sightseeing car supercapacitor charge," *IEEE Trans. Power Electron.*, vol. 32, no. 5, pp. 3301–3316, May 2017.

[13] Z. Ding, C. Yang, Z. Zhang, C. Wang, and S. Xie, "A novel soft-switching multiport bidirectional DC–DC converter for hybrid energy storage system," *IEEE Trans. Power Electron.*, vol. 29, no. 4, pp. 1595–1609, Apr. 2014.

[14] M. E. Choi, J. S. Lee, and S. W. Seo, "Real-time optimization for power management systems of a battery/supercapacitor hybrid energy storage system in electric vehicles," *IEEE Trans. Veh. Technol.*, vol. 63, no. 8, pp. 3600–3611, Oct. 2014.

[15] D. B. W. Abeywardana, B. Hredzak, and V. G. Agelidis, "Single-phase grid-connected LiFePO4 battery–supercapacitor hybrid energy storage system with interleaved boost inverter," *IEEE Trans. Power Electron.*, vol. 30, no. 10, pp. 5591–5604, Oct. 2015.

[16] W. Jing, C. Hung Lai, S. H. W. Wong, and M. L. D. Wong, "Battery-supercapacitor hybrid energy storage system in standalone DC microgrids: A review," *IET Renewable Power Gener.*, vol. 11, no. 4, pp. 461 469, 2017.

[17] O. Gomozov, J. P. F. Trovão, X. Kestelyn, and M. R. Dubois, "Adaptive power management system based on a real-time model predictive control with nonuniform sampling time for multiple energy storage electric vehicle," *IEEE Trans. Veh. Technol.*, vol. 66, no. 7, pp. 5520–5530, Jul. 2017.

[18] B. Wang, J. Xu, R. J. Wai, and B. Cao, "Adaptive sliding-mode with hysteresis control strategy for simple multimode hybrid energy storage system in electric vehicles," *IEEE Trans. Ind. Electron.*, vol. 64, no. 2, pp. 1404–1414, Feb. 2017.

[19] J. Shen and A. Khaligh, "Design and real-time controller implementation for a battery-ultracapacitor hybrid energy storage system," *IEEE Trans. Ind. Informat.*, vol. 12, no. 5, pp. 1910–1918, Oct. 2016.

[20] D. B. W. Abeywardana, B. Hredzak, and V. G. Agelidis, "A fixed-frequency sliding mode controller for a boost-inverter-based battery-supercapacitor hybrid energy storage system," *IEEE Trans. Power Electron.*, vol. 32, no. 1, pp. 668–680, Jan. 2017.

[21] C. Zhao, H. Yin, and C. Ma, "Quantitative efficiency and temperature analysis of battery-ultracapacitor hybrid energy storage systems," *IEEE Trans. Sustain. Energy*, vol. 7, no. 4, pp. 1791–1802, Oct. 2016.

[22] Y. D. Lee and S. Y. Park, "Electrochemical state-based sinusoidal ripple current charging control," *IEEE Trans. Power Electron.*, vol. 30, no. 8, pp. 4232–4243, Aug. 2015.

[23] W. Zhang, J. C. White, A. M. Abraham, and C. C. Mi, "Loosely coupled transformer structure and interoperability study for EV wireless charging systems," *IEEE Trans. Power Electron.*, vol. 30, no. 11, pp. 6356–6367, Nov. 2015.

[24] V. Jiwariyavej, T. Imura, and Y. Hori, "Coupling coefficients estimation of wireless power transfer system via magnetic resonance coupling using information from either side of the system," *IEEE J. Emerg. Sel. Topics Power Electron.*, vol. 3, no. 1, pp. 191–200, Mar. 2015.
[25] T. Imura and Y. Hori, "Maximizing air gap and efficiency of magnetic resonant coupling for wireless power transfer using equivalent circuit and Neumann formula," *IEEE Trans. Ind. Electron.*, vol. 58, no. 10, pp. 4746–4752, Oct. 2011.
[26] Z. Bi, T. Kan, C. C. Mi, Y. Zhang, Z. Zhao, and G. A. Keoleian, "A review of wireless power transfer for electric vehicles: Prospects to enhance sustainable mobility," *Appl. Energy*, vol. 179, pp. 413–425, 2016.
[27] T. Kan, T. D. Nguyen, J. C. White, R. K. Malhan, and C. C. Mi, "A new integration method for an electric vehicle wireless charging system using LCC compensation topology: Analysis and design," *IEEE Trans. Power Electron.*, vol. 32, no. 2, pp. 1638–1650, Feb. 2017.
[28] J. Deng, F. Lu, S. Li, T. D. Nguyen, and C. Mi, "Development of a high efficiency primary side controlled 7kW wireless power charger," in *Proc. Int. Elect. Veh. Conf.*, 2014, pp. 1–6.
[29] S. Li, W. Li, J. Deng, T. D. Nguyen, and C. C. Mi, "A double-sided LCC compensation network and its tuning method for wireless power transfer," *IEEE Trans. Veh. Technol.*, vol. 64, no. 6, pp. 2261–2273, Jun. 2015.
[30] W. Li, H. Zhao, J. Deng, S. Li, and C. C. Mi, "Comparison study on SS and double-sided LCC compensation topologies for EV/PHEV wireless chargers," *IEEE Trans. Veh. Technol.*, vol. 65, no. 6, pp. 4429–4439, Jun. 2016.

Jia-Sheng Hu (S'04–M'07–SM'15) received the B.S. degree in electrical engineering from the National Taiwan Ocean University, Keelung, Taiwan, in 2001, and the M.S. and Ph.D. degrees in system and control division from the Department of Mechanical Engineering, National Cheng Kung University, Keelung, Taiwan, in 2003 and 2007, respectively.

He was a Postdoctoral Fellow and a Project Assistant Professor with the University of Tokyo in 2008 and 2014, respectively. In 2009, he was a Visiting Research Scholar with the California Institute of Technology. He is currently an Associate Professor with the Department of Greenergy, National University of Tainan, Tainan, Taiwan, performing research on the development of motion control for electric vehicles. His research interests include electric vehicle, motion control, and robotics.

Dr. Hu is a member of SAE Taipei Section, Asian Control Association, and Phi Tau Phi Scholastic Honor Society.

Fei Lu (S'12–M'17) received the M.S. and B.S. degree from the Harbin Institute of Technology, Harbin, China, in 2010, and 2012, respectively, and the Ph.D. degree from the University of Michigan, Ann Arbor, MI, USA, in 2017, all in electrical engineering.

His research interests include wireless power transfer for the application of electric vehicle charging. He is working on the high-power and high-efficiency capacitive power transfer through an air-gap distance up to 100's of millimeters. He is also working on the application of wide band-gap devices on WPT system to increase the system frequency.

Chong Zhu (M'17) received the B.S. degree from the China University of Mining and Technology, Xuzhou, China, in 2010, and the Ph.D. degree from Zhejiang University, Hangzhou, China, in 2016, both in electrical engineering.

He is currently holding a postdoctoral position with San Diego State University, San Diego, CA, USA. His research interests include modeling, control, and modulation techniques of power converters and motor drives. He is also working on the battery thermal management in hybrid electric vehicles.

Chang-Yi Cheng received the B.S. degree in energy and system division from the Department of Greenergy, National University of Tainan, Tainan, Taiwan, in 2017.

He is currently a master course student with the Department of Electrical Engineering, National Cheng Kung University, Tainan, Taiwan. His research interests include hybrid energy storage management, wireless power transfer for electric vehicles, and driving control of permanent-magnet synchronous motor.

Sin-Li Chen received the B.S. degree from the Department of Information Engineering, Kun Shan University, Tainan, Taiwan, in 2014, and received the M.S. degree from the Department of Greenergy, National University of Tainan, Tainan, Taiwan, in 2016.

His research interests include microcontroller, energy storage system, and wireless power transfer for electric vehicles.

Tsai-Jiun Ren received the B.S, M.S., and Ph.D. degrees from the Department of Engineering Science, National Cheng Kung University, Tainan, Taiwan, in 1999, 2001, and 2007, respectively.

He is currently an Associate Professor with the Department of Information Engineering, Kun Shan University, Tainan, Taiwan, performing research on the development of intelligent control for robot. His research interests include impendence control, motion control, and green energy conversion.

Chunting Chris Mi (S'00–A'01–M'01–SM'03–F'12) received the B.S.E.E. and M.S.E.E. degrees from the Northwestern Polytechnical University, Xi'an, China, and the Ph.D. degree from the University of Toronto, Toronto, ON, Canada, in 1985, 1988, and 2001, respectively, all in electrical engineering.

He is currently a Professor and the Chair of electrical and computer engineering and the Director of the Department of Energy-funded Graduate Automotive Technology Education, Center for Electric Drive Transportation, San Diego State University (SDSU), San Diego, CA, USA. Prior to joining SDSU, he was with University of Michigan, Dearborn, MI, USA, from 2001 to 2015. He was the President and the Chief Technical Officer of 1Power Solutions, Inc., from 2008 to 2011. He is the cofounder of Gannon Motors and Controls LLC, San Diego, CA, USA, and Mia Motors, Inc., San Diego, CA, USA. His research interests include electric drives, power electronics, electric machines, renewable-energy systems, and electrical and hybrid vehicles.

Prof. Mi is a Fellow of SAE.